Biophysical Chemistry 144 (2009) 38–45

Contents lists available at ScienceDirect

Biophysical Chemistry

journal homepage: http://www.elsevier.com/locate/biophyschem

DNA-binding geometry dependent energy transfer from 4′,6-diamidino-2-phenylindole to cationic porphyrins

Biao Jin [a], Kil Sik Min [b], Sung Wook Han [c], Seog K. Kim [a,*]

[a] Department of Chemistry, Yeungnam University, Gyeongsan City, Gyeongbuk, 712-749, Republic of Korea
[b] Department of Chemistry Education, Kyungpook National University, Daegu City, 702-701, Republic of Korea
[c] School of Herb Medicine Resource, Kyungwoon University, Sangdong-myeon, Gumi, Gyeongbuk, 730-739, Republic of Korea

ARTICLE INFO

Article history:
Received 9 April 2009
Received in revised form 6 June 2009
Accepted 9 June 2009
Available online 16 June 2009

Keywords:
DNA
Porphyrin
4′,6-Diamidino-2-phenylindole
Energy transfer
Luminescence

ABSTRACT

The circular and linear dichroism (CD and LD) spectral properties of the *meso*-tetrakis(*N*-methylpyridinium-4-yl)porphyrin (TMPyP)–DNA complex at a [porphyrin]/[DNA] ratio below 0.015 showed that TMPyP intercalates between DNA base pairs. Contrarily, when *cis*–*bis*(*N*-methylpyridinium-4-yl)porphyrin (BMPyP) is associated with DNA, no CD spectrum was induced and a bisignate LD spectrum was observed. These spectral properties of both the TMPyP and BMPyP were essentially retained when the minor groove of the DNA was saturated with 4′,6-diamidino-2-phenylindole (DAPI). The fluorescence of the DNA-bound DAPI was effectively quenched by BMPyP and TMPyP. The quenching by BMPyP can be described through a pure static mechanism while TMPyP quenching produced an upward bending curve in the Stern–Volmer plot. Quenching efficiency was by far greater than predicted by the "sphere of action model", suggesting that the DNA provides some additional processes for an effective energy transfer.

1. Introduction

Energy and charge transfer along DNA has been a subject of intense study since the stacked π-orbitals of DNA base pairs were found to be an effective medium for electron and hole transfer [1–7]. The biological importance of charge transport has been highlighted by the discovery of distance oxidative damage to DNA in the cell nucleus [8,9]. As an early example of electron transport through DNA [10,11], the luminescence intensity of the DNA intercalating [Ru(1,10-phenanthroline)$_2$dypyrido[3,2-*a*:2′3′-*c*]phenazine]$^{2+}$ (hereafter referred to as [Ru(phen)$_2$dppz]$^{2+}$) was efficiently quenched by a [Rh(9,10-diimine phenanthrenequinone)$_2$phenanthrolone]$^{3+}$ complex through an electron transfer mechanism. Nevertheless, quenching efficiency was significantly lowered when the DNA was modified with [Ru(NH$_3$)$_6$]$^{3+}$. The former quencher intercalates between the DNA base pairs while the latter binds at the DNA surface, thus supporting electron transfer through the stacked π-orbitals of the DNA base pairs. Currently, three basic mechanisms have been suggested for photo-induced electron transfer through DNA: the molecular wire; the superexchange mechanism; and the hopping model [6]. Hole transfer has also been reported [12–16]. For instance, hole injection into guanines of different oligonucleotide duplexes by a tethered Ru(II) complex has been reported, whereby the tethered Ru(II) complex absorbed into the duplex grooves and provided the close contact between the complex and guanine base required for hole transfer.

Charge transport between a donor and acceptor molecule through DNA is usually accompanied by an energy transfer, which is often revealed as the quenching of the fluorescence of the donor molecule by the presence of the acceptor molecule. Fluorescence quenching through a Förster type energy transfer between the DNA-bound donor and acceptor molecules has been investigated [17–21]. For instance, the excitation energy of 4′,6-diamidino-2-phenylindole (hereafter referred to as DAPI, Fig. 1), a DNA minor groove-binding drug [22–27], is transferred to [Ru(phen)$_2$dppz]$^{2+}$ or *meso*-tetrakis(*N*-methylpyridinium-4-yl)porphyrin (hereafter referred to as TMPyP, Fig. 1) at a high binding density. In the former case, the dypyrido[3,2-*a*:2′3′-*c*]phenazine (dppz) ligand intercalates between the DNA base pair from the major groove as the minor groove is saturated by DAPI [17,18], thus, the energy transfer occurs eventually across the DNA. Conversely, in the latter case, the excitation energy of the poly(dA)·poly(dT)- and poly[d(A-T)$_2$]-bound DAPI transferred efficiently to TMPyP, which has been previously suggested to bind across the minor groove of poly(dA)·poly(dT) and poly[d(A-T)$_2$] [19].

In this work, the efficiency of the energy transfer between the DNA-bound DAPI and two porphyrins, namely TMPyP and *cis*–*bis*(*N*-methylpyridinium-4-yl)porphyrin (hereafter referred to as BMPyP, Fig. 1) is investigated. In contrast to poly[d(A-T)$_2$] and poly(dA)·poly(dT), TMPyP has been known to intercalate between base pairs of native DNA, poly[d(G-C)$_2$] and poly(dG)·poly(dC) at a low [porphyrin]/[DNA] ratio [28–32], while BMPyP potentially stacks in the major groove of DNA. Thus, this study may provide information regarding the effects of the binding mode of the acceptor molecules on energy transfer along DNA, which may accompany electron transfer.

* Corresponding author. Tel.: +82 53 810 2362; fax: +82 53 815 5412.
E-mail address: seogkim@ynu.ac.kr (S.K. Kim).

0301-4622/$ – see front matter © 2009 Elsevier B.V. All rights reserved.
doi:10.1016/j.bpc.2009.06.003

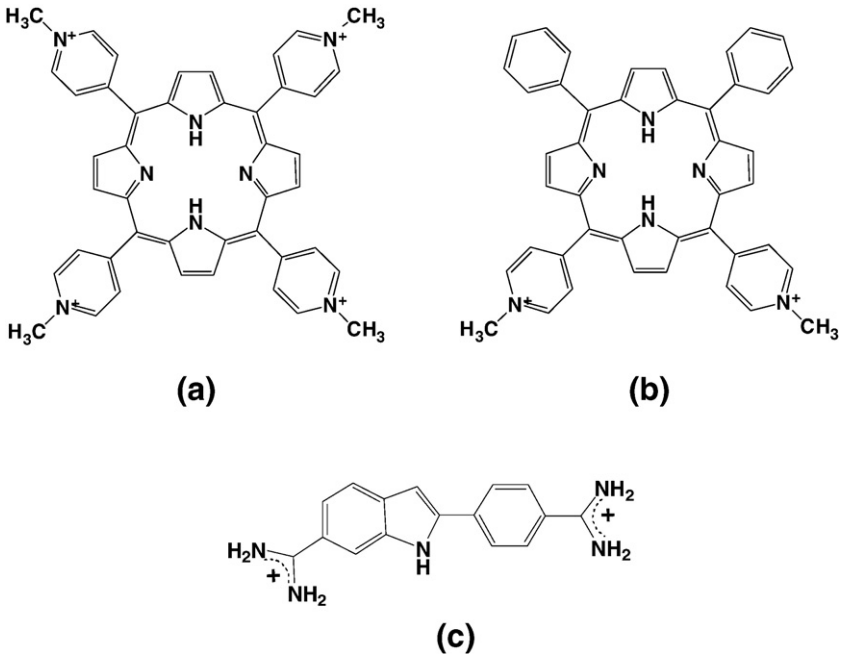

Fig. 1. Chemical structures of: (a) *meso*-tetrakis(*N*-methylpyridinium-4-yl)porphyrin (TMPyP); (b) *cis*–*bis*(*N*-methylpyridinium-4-yl)porphyrin (BMPyP); (c) 4′,6-diamidino-2-phenylindole (DAPI).

The effect of blocking the minor groove with DAPI on the binding mode of TMPyP and BMPyP was also investigated.

2. Materials and methods

2.1. Materials

Calf thymus DNA ($\varepsilon_{260\ nm} = 6700\ cm^{-1}\ M^{-1}$), purchased from Worthington Biochem. Co. (Lakewood, NJ, USA), was dissolved in 5.0 mM cacodylate buffer (pH 7.0), containing 100 mM NaCl and 1.0 mM EDTA, by exhaustive shaking at 4 °C, followed by several dialyses against 5.0 mM cacodylate buffer (pH 7.0). The latter buffer solution was used throughout this work. The concentration of DNA, therefore, denotes the DNA concentration in base or phosphate. TMPyP ($\varepsilon_{421\ nm} = 2.45\times10^5\ cm^{-1}\ M^{-1}$) and BMPyP ($\varepsilon_{419\ nm} = 1.4\times10^5\ cm^{-1}\ M^{-1}$) [33,34] were purchased from Frontier Scientific, Inc.(Logan, UT, USA) and DAPI ($\varepsilon_{342\ nm} = 2.7\times10^4\ cm^{-1}\ M^{-1}$) from Sigma-Aldrich (St. Louis, MO, USA) and used without further purification. Throughout this work, the DNA concentration was either 200 μM (for absorption, and circular and linear dichroism measurements) in base or phosphate (or 100 μM in base pair) or 20 μM (for fluorescence measurements). The [DAPI]/[DNA] ratio was maintained at 0.2, corresponding to one DAPI molecule per five DNA base pairs [22,24], at which the minor groove of DNA was nearly saturated. The spectral properties of DNA-bound porphyrin can be affected by the order of mixing [35], thus, the porphyrin was added last every time.

2.2. Measurement

The steady state fluorescence intensity of the DNA–DAPI complex was measured at 360 and 456 nm for excitation and emission, using a Jasco FP777 spectrofluorometer. Slit widths were 5 nm for both excitation and emission. An upward bending curve in the Stern–Volmer plot was observed in the quenching of the DNA-binding DAPI fluorescence by porphyrins (see Results section). This type of quenching may be interpreted in terms of the sphere of action model, whereby within the sphere, the probability of quenching is unity [36]:

$$\frac{F_0}{F} = (1 + K_D[Q])\exp([Q]VN/1000) \quad (1)$$

where K_D is the dynamic quenching constant, and V and N denote the volume of the sphere and Avogadro's number, respectively. Fluorescence decay times were measured using an IBH 5000U Fluorescence Life Time System. The LED source of a nanoLED-03, which produces an excitation radiation at 370 nm with a full width at half maximum of ~1.3 ns, was used to excite DAPI bound to DNA. The fluorescence intensity of the DNA–DAPI complex in the presence and absence of the porphyrins was monitored through 460 nm emissions. The respective slit widths for excitation and emission were 8 and 12 nm.

Absorption spectra were recorded on a Cary 100 Bio spectrophotometer (Victoria, Australia), circular dichroism spectra (hereafter CD) on a Jasco J810 spectropolarimeter, and linear dichroism (referred to as LD) on a Jasco J715 spectropolarimeter (Tokyo, Japan). LD is the difference in the absorption of polarized parallel and perpendicular radiation relative to the laboratory reference axis of an oriented sample. The measured LD is divided by the isotropic absorption spectrum, resulting in the reduced LD spectrum (referred to as LD^r), which relates to the angle, α, between the electronic transition moments of the DNA-bound drugs to the local DNA helical axis as follow [37–39].

$$LD^r = \frac{LD}{A_{iso}} = 1.5S\left(<3\cos^2\alpha> - 1\right) \quad (2)$$

where the orientation factor, S, reflects the ability of the orientation of the sample." The LD spectra were recorded using a Wada-type inner rotating Couette cell device [40] using a previously published method [19].

3. Results

3.1. Fluorescence measurement

It has been reported that the fluorescence intensity of DAPI increases in large extent upon binding to the minor groove of native DNA or synthetic AT-rich DNAs [41,42]. The increase is almost proportional to the [DAPI]/[DNA] ratio, up to 0.2, at which point DAPI saturates the minor groove. When the DAPI concentration exceeds the saturation point, fluorescence intensity starts to decrease due to self-quenching. Upon addition of TMPyP or BMPyP, the fluorescence intensity of the DNA–DAPI adduct is quenched (Fig. 2, inset). The decrease in fluorescence intensity of the complex at the maximum wavelength with respect to the concentration of the BMPyP is depicted in the Stern–Volmer plot (Fig. 2a). Within the range of the BMPyP concentration adopted in this work, up to 0.3 μM, corresponding to a [porphyrin]/[DNA] ratio of 0.015, the Stern–Volmer plot appeared to be a straight line. The fluorescence decay time of the DNA–DAPI complex in the absence of BMPyP was 1.01 and 3.08 ns, with relative amplitudes of $a_1 = 0.36$ and $a_2 = 0.64$, respectively, and all in agreement with reported values [43–45]. The presence of BMPyP did not alter the decay profile. For instance, the fluorescence decay time of the DNA–DAPI complex was 0.89 ns ($a_1 = 0.34$) and 2.98 ns ($a_2 = 0.66$) in the presence of 0.3 μM BMPyP. The average life-times, defined by: $\tau = (a_1\tau_1^2 + a_2\tau_2^2)/(a_1\tau_1 + a_2\tau_2)$ [36], were 2.76 and 2.70 ns in the absence and presence of BMPyP, respectively. This observation suggests that the quenching of the DNA–DAPI complex by BMPyP is static in nature, such as the decrease in fluorescence intensity by forming a non-fluorescent complex. The static quenching constant, often considered the equilibrium constant for the formation of the non-fluorescent complex, was $3.63 \times 10^5\ M^{-1}$. In contrast to BMPyP, an upward bending curve was observed in the Stern–Volmer plot when TMPyP was used as a quencher (Fig. 2b). Upon increasing the TMPyP concentration, the fluorescence decay time of the DNA–DAPI complex shortened, suggesting the quenching mechanism is not straightforward, which is also in contrast with BMPyP. In the presence of TMPyP the fluorescence decay time of the DNA–DAPI complex was 0.79 ns ($a_1 = 0.38$) and 2.83 ns ($a_2 = 0.62$) in the presence of 0.3 μM TMPyP. When the ratio of the average fluorescence decay time of the DNA–DAPI complex with respect to the TMPyP concentration is plotted, a straight line was observed with a dynamic quenching constant of $3.29 \times 10^5\ M^{-1}$. Given the dynamic quenching constant K_D, a sphere radius of ~840 Å was obtained from Eq. (1). The sphere radius in the sphere of action model, within which the quenching efficiency is unity, is in a range comparable to the sum of radii of the fluorophore and quencher [46]. Thus, the value of the sphere radius obtained in this study is unrealistically large.

It is noted as worthy that the emission band of the DNA-bound DAPI and the porphyrin's Soret absorption band overlap to a large extent. Hence, the mechanism behind the quenching of the DNA–DAPI complex by both porphyrins involves, at least in part, a Förster type resonance energy transfer. If this is indeed the case, efficiency in fluorescence decreasing by forming a non-fluorescent DAPI–porphyrin complex may depend on wavelength. In other words, more effective quenching in the porphyrin absorption region would be expected. Fig. 3a shows the ratio

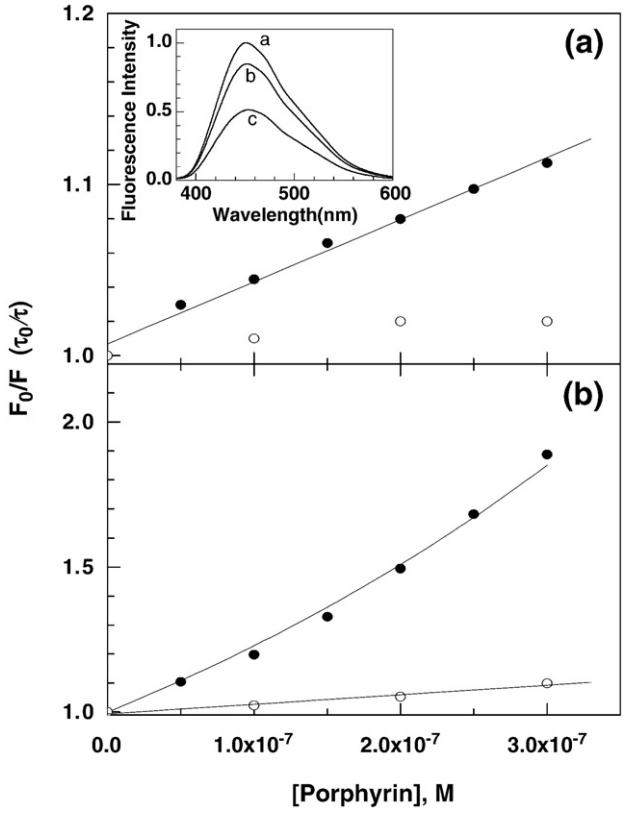

Fig. 2. (a) The Stern–Volmer plot for the fluorescence quenching of the DNA–DAPI complex by BMPyP (solid circles). The fluorescence decay times are marked by open circles. Inset: Fluorescence emission spectrum of the DNA–DAPI complex (curve a), in the presence of BMPyP (curve b), and TMPyP (curve c). (b) Stern–Volmer plot for the quenching by TMPyP. The solid curve is the best-fit curve for the equation $F_0/F = (1 + K_D[Q]\exp([Q]VN/1000)$ (see text for the appropriate values of K_D and V). Changes in the fluorescence decay times by TMPyP (τ_0/τ) versus [TMPyP] appear as open circles. [DNA] = 20 μM and [DAPI] = 2.0 μM. Fluorescence was measured at an excitation wavelength of 360 nm and emission wavelength of 456 nm. The slit for both excitation and emission was 5 nm.

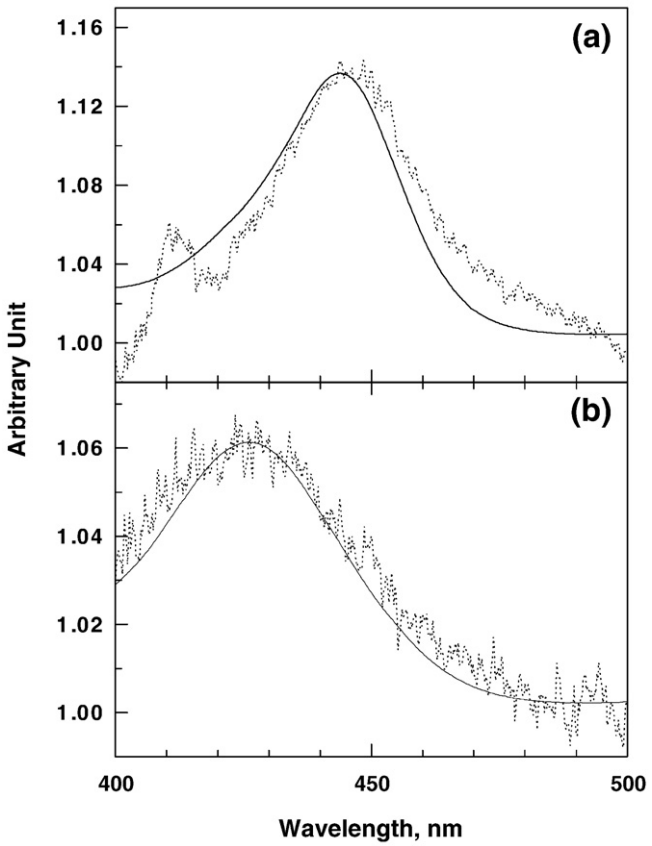

Fig. 3. The ratio of the fluorescence emission spectrum of the DNA–DAPI complex in the absence of porphyrin to its presence (dotted curve). The spectra were multiplied by −1 and normalized at 500 nm, outside of the Soret region, for ease of comparison. The rescaled absorption spectrum of porphyrin, obtained by subtracting the absorption spectrum of the DNA–DAPI complex from the DNA–DAPI–TMPyP complex, is compared. [DNA] = 20 μM, [DAPI] = 2.0 μM, and [porphyrin] = 0.3 μM. Panel (a) in the presence of TMPyP and (b) of BMPyP.

of the fluorescence emission spectrum of the DNA–DAPI complex in the absence of TMPyP to its presence. For ease of comparison, the wavelength-dependent ratio was normalized at 500 nm, outside the Soret absorption envelop. The rescaled absorption spectrum of TMPyP, obtained by subtracting the absorption spectrum of the DNA–DAPI complex from the DNA–DAPI–TMPyP complex, is comparable. The quenching of the DNA–DAPI complex fluorescence by TMPyP is most efficient at 446 nm and coincides with the absorption maximum of TMPyP at 444 nm. The overall shape of the wavelength-dependent quenching efficiency also coincides with the shape of the absorption spectrum of bound TMPyP. This observation supports the involvement of the Förster type resonance energy transfer in the quenching mechanism. Involvement of the Förster type resonance energy transfer is clear in the case of BMPyP. When a similar spectrum was constructed, the shape of the absorption and wavelength-dependent quenching efficiency was nearly identical (Fig. 3b), with the maximum at 427 nm.

The aforementioned fluorescence of the DNA–DAPI complex was measured at 360 and 456 nm for excitation and emission, respectively, where porphyrin fluorescence is negligible. Thus, the fluorescence intensity discussed in this section is solely from the DNA-bound DAPI. It should also be noted that no quenching activity in the absence of DNA was observed for BMPyP or TMPyP, and thus the quenching of DAPI by BMPyP and TMPyP occurred only when they bound simultaneously to DNA.

3.2. Absorption and CD

The absorption spectrum of the DNA–DAPI–TMPyP system is depicted in Fig. 4a. The absorption spectrum of the DNA–DAPI complex in the DAPI absorption region, 300–400 nm, was identical in both the absence and presence of TMPyP, such as a computer sum of

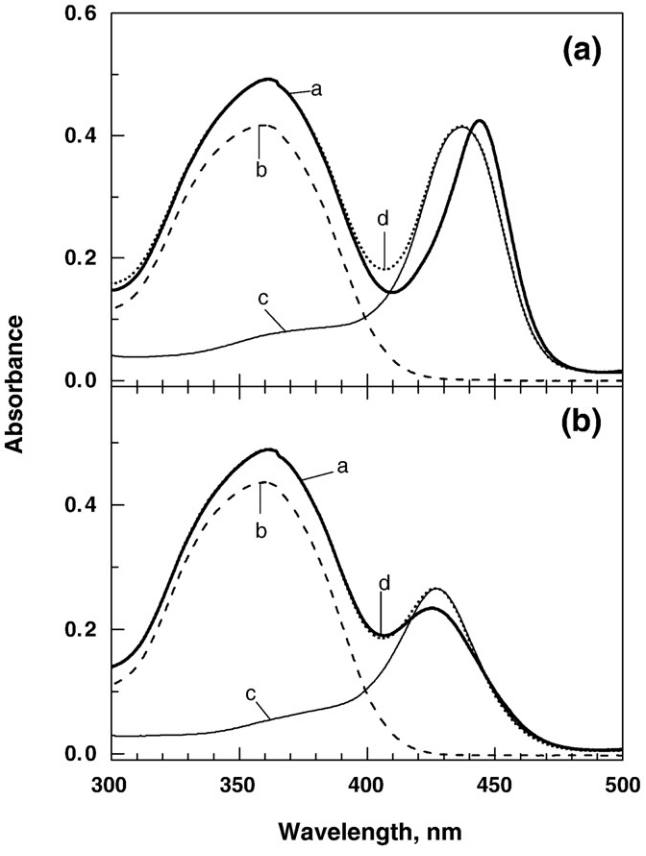

Fig. 4. Absorption spectrum of the DNA–DAPI–porphyrin (curve a, thick solid), DNA–DAPI (curve b, dashed), DNA–porphyrin (curve c, thin solid), and computer generated sum of curves b and c (curve d, dotted). Panel a: TMPyP and panel b: BMPyP. [DNA] = 200 μM, [DAPI] = 20 μM and [porphyrin] = 3.0 μM.

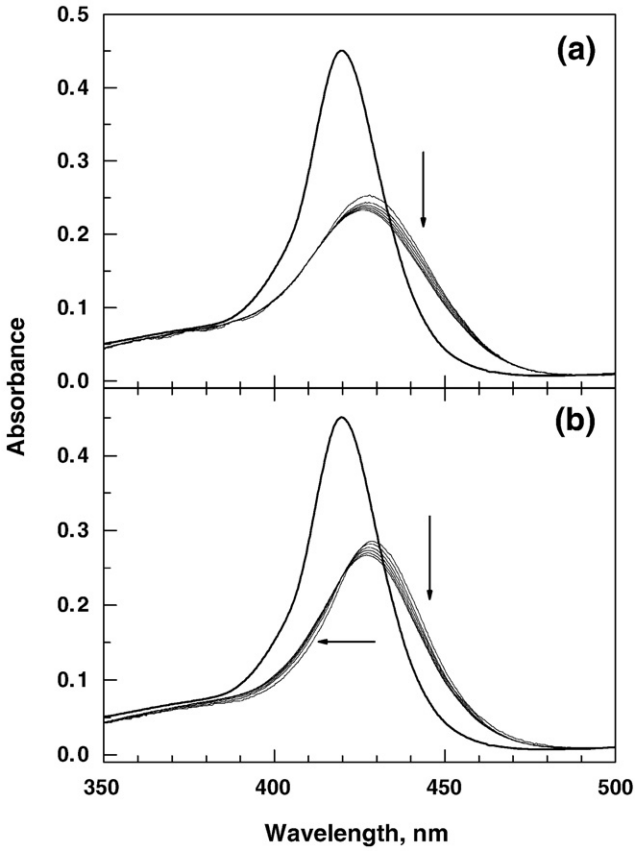

Fig. 5. Absorption spectrum of BMPyP associated with DNA (panel a) and the DNA–DAPI complex (panel b) at various concentrations. [DNA] = 200 μM, [DAPI] = 20 μM, and [BMPyP] = 0.5, 1.0, 1.5, 2.0, 2.5 and 3.0 μM to the direction of arrow. Absorption spectra were normalized to the highest concentration for ease of comparison.

the absorption spectrum of the DNA–DAPI and DNA–TMPyP complex was identical to the measured absorption spectrum of the DNA–DAPI–TMPyP complex, suggesting that the binding mode of DAPI to DNA was unaltered by the presence of TMPyP. However, some differences in the Soret band were observed, whereby an absorption maximum (437 nm) of the DNA–TMPyP complex shifted to 444 nm in the presence of DAPI. The absorption spectrum of TMPyP whether bound to DNA or the DNA–DAPI complex, was invariant of the mixing ratio when normalized to concentration (data not shown). The absorption spectrum of the DNA–DAPI complex in the 300–400 nm region also remained unchanged in the presence of BMPyP (Fig. 4b), while that of the Soret band was altered. The absorption maximum of the DNA-bound BMPyP was found at 427 nm at the highest BMPyP concentration (3.0 μM). This maximum wavelength did not shift, even in the presence of DAPI. However, a decrease in the maximum absorbance was observed in the presence of DAPI. In contrast to TMPyP, the absorption spectrum of the DNA–BMPyP complex in the Soret band changed with increasing BMPyP concentration whether in the presence or absence of DAPI (Fig. 5).

Fig. 6a shows the induced CD spectrum of the DNA–DAPI, DNA–TMPyP, and DNA–DAPI–TMPyP complexes. CD in the DAPI absorption region was positive with its maximum at 368 nm, as previously reported [22,23,42], and was unaltered by the presence of TMPyP. A negative CD band with a minimum at 446 nm, known as a diagnostic marker for intercalation of porphyrin to DNA, was antipodal to cases involving poly[d(A-T)$_2$]–DAPI–TMPyP and poly[d(A-T)$_2$]–TMPyP complexes at similar concentrations [19]. The magnitude of this negative CD signal in the Soret region increased in the presence of DAPI, but the negative nature remained the same. The CD spectrum of the DNA-bound BMPyP in the Soret region was extremely weak within

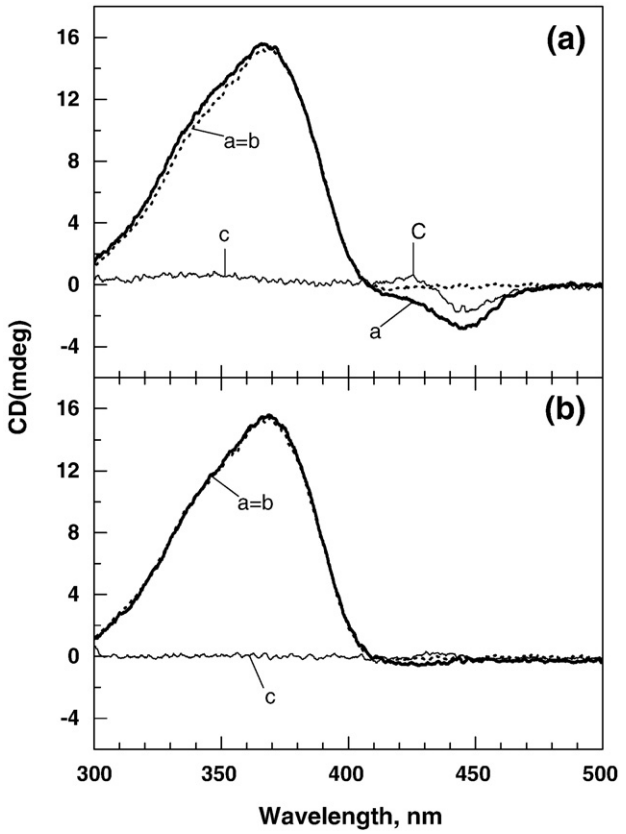

Fig. 6. CD spectrum the DNA–TMPyP (panel a) and –BMPyP (panel b) complex in the presence and absence of DAPI. Curve a (thick solid): in the presence of DAPI; curve c (thin solid): in the absence of DAPI; curve c (dotted): DNA–DAPI in the absence of porphyrin. [DNA] = 200 μM, [DAPI] = 20 μM and TMPyP = 3.0 μM. Panel b depicts the CD spectrum of BMPyP. Curve assignment and concentration are the same as in panel a.

the concentration adopted in this study (Fig. 6b) whether in the presence or absence of DAPI. Similar to TMPyP, the CD spectrum in the DAPI absorption region, consisting of a strong positive band, was not affected by the presence of BMPyP.

3.3. LD and LD^r

The LD spectra of the DNA–DAPI–TMPyP and DNA–DAPI–BMPyP systems at their maximum concentrations ([DNA] = 200 μM, [DAPI] = 20 μM, [porphyrin] = 3.0 μM) are depicted in Fig. 7a and b, respectively. As expected from the set-up, a negative band in the DNA absorption region (200–300 nm) was apparent for all cases with a minimum near 258 nm, suggesting that the average orientation of the DNA bases was near perpendicular relative to the flow direction. A positive band in the DAPI absorption region (300–400 nm) for the DNA–DAPI and DNA–DAPI–porphyrin complexes suggested that the long axis of the electronic transition moment of DAPI, which lies along the bond connecting the phenyl and indole groups, tilts strongly with respect to the local DNA helical axis. In the Soret band, a large negative band with its minimum near 444 nm was observed for the DNA-bound TMPyP, whether DAPI is present or not. A similar negative signal in the DNA absorption region and the positive DAPI absorption region was observed in the BMTyP system. However, a bisignate LD spectrum with its positive maximum at 419 nm and negative minimum at 447 nm was observed for the DNA-bound BMPyP, which is in contrast with TMPyP, suggesting that the geometries of BMPyP and TMPyP were different when bound to DNA.

The LD^r spectra of the DNA–TMPyP and DNA–BMPyP complexes are depicted in Fig. 8a. In the case of TMPyP, a negative LD^r in the Soret absorption region, whose wavelength-dependent magnitude was larger than that in the DNA absorption region, was apparent and is typical for intercalated drugs. For TMPyP, wavelength-dependency may be attributed to the different angles of the two electronic transition moments, namely B_x and B_y, relative to the local DNA helical axis (orientation axis). As discussed below, a detailed analysis of the LD^r spectrum resulted in the LD^r magnitude representing B_x and B_y transition moments larger than that in the DNA absorption region, reflecting that the molecular plane is near perpendicular with respect to the DNA helical axis. The case of BMPyP is quite different from TMPyP though. The LD^r magnitude in the Soret band is bisignate, as expected from the measured LD spectrum. This observation, indicates that the binding geometry of BMPyP is in sharp contrast with that of TMPyP. When DAPI is associated with DNA, it locates along the minor groove of the DNA, resulting in an angle of approximately 45° between the long axes of the DAPI and the local DNA helical axis, producing a positive LD^r in the DAPI absorption region (Fig. 8b) [22,42]. Binding of TMPyP to the DNA–DAPI complex resulted in a small decrease in the DAPI absorption region that may be attributed either to the negative contribution from TMPyP or the small change in the binding angle of DAPI. However, the variation in angle between the long axis of DAPI and the local DNA helical axis calculated from the LD^r at 350 nm was negligible. Here, the angle is 45° for the DNA–DAPI complex and 47° and 48° in the presence of BMPyP and TMPyP, respectively. The properties of the LD^r spectra of TMPyP and BMPyP in the presence of DAPI remain essentially the same. For the TMPyP, the LD^r in the Soret region is characterized by a wavelength-dependent negative LD^r whose magnitude is larger than the DNA absorption region. Contrarily, it is bisignated for BMPyP suggesting that the binding geometry of the

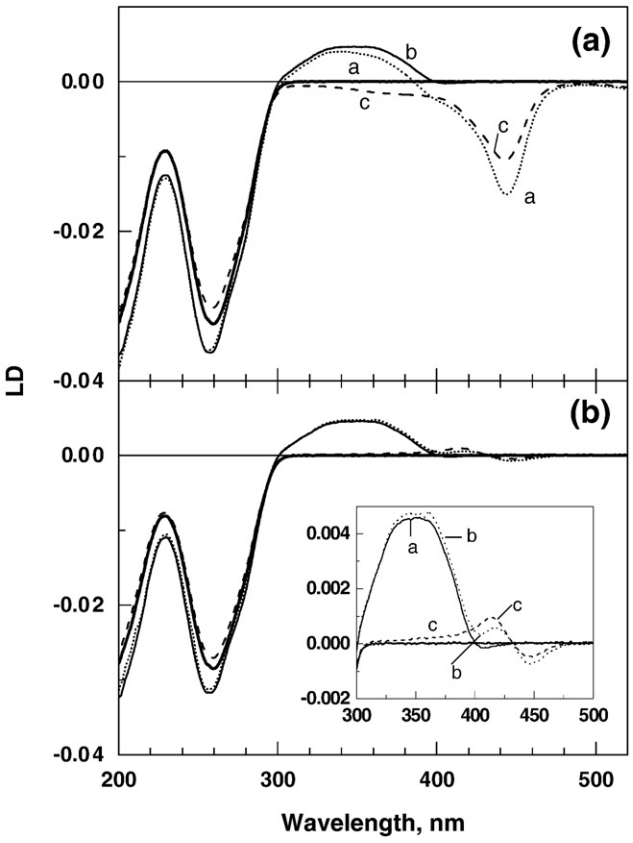

Fig. 7. LD spectrum of the DNA–TMPyP (panel a) and –BMPyP (panel b) complex in the presence and absence of DPAI. Curve a (dotted): in the presence of DAPI, curve c (dashed): in the absence of DAPI; curve c (solid): DNA–DAPI in the absence of porphyrin. The enlarged spectrum is inserted in panel b. [DNA] = 200 μM, [DAPI] = 20 μM and TMPyP = 3.0 μM. Panel b depicts the LD spectrum of BMPyP. Curve assignment and concentration are the same as in panel a.

DAPI remains, even when the porphyrins are bound, and that of the porphyrins are little affected by the presence of DAPI.

The LD spectrum can be further analyzed in some DNA–porphyrin adduct cases [19,47]. The degeneracy of the two electronic transition moments in the Soret band, B_x and B_y, in the absorption and LD spectrum can be, at least partially, removed by having different interactions and angles relative to the local DNA helical axis. The absorption and LD spectra are the sum of contributions of the two transitions, which allows the pure contribution of the B_y transition in the LD spectrum ($LD_{B_y}(\lambda)$) to be obtained by stepwise reduction of the properly tuned absorption spectrum from the LD spectrum:

$$LD_{B_y}(\lambda) = LD(\lambda) - \kappa A(\lambda) \tag{3}$$

Fig. 9b depicts the absorption spectrum and LD spectrum, multiplied by 10, for the DNA–BMPyP complex at a [porphyrin]/[DNA] ratio of 0.015 ([DNA] = 200 μM). Curves in Fig. 9b show the $LD(\lambda) - \kappa A(\lambda)$ spectrum with the various κ values ranging from −0.02 and −0.10, at increments of 0.02. The spectrum obtained from the κ value of −0.08 was chosen as representative of the $LD_{B_y}(\lambda)$. This correspondence to $LD_{B_y}(\lambda)$ can be deduced by subtracting the $LD_{B_y}(\lambda)$ spectrum from the measured LD. In a similar method, the absorption spectrum can also be resolved through the sum of two absorption spectra. The LD^r values corresponding to B_x and B_y transitions can be obtained from resolved absorption and LD spectra. The S value in Eq. (2) is calculated by assuming an average angle of 86° between the DNA base plane relative to the local DNA helical axis and the LD^r value at 258 nm. Given the S and the LD^r values, the angles of B_x and B_y relative to the local DNA helix axis were calculated as ~40° and ~60° for the DNA–BMPyP complex at a [porphyrin]/[DNA] ratio of 0.015. From these angles, the possibility of intercalation of BMPyP into DNA can be ruled out with certainty. Similar results, although with little variation in the angles, were obtained from the DNA–BMPyP complex at low mixing ratios (data not shown). In the DNA–TMPyP complex, similar approaches resulted in LD^r values of B_x and B_y transitions larger than those in the DNA absorption region that prevented the calculation of the precise angles given the involvement of imagery numbers. However, average angles between the DNA base plane and transition moments of the TMPyP can be calculated by taking the largest LD^r value as the reference, which was found at 430 nm, corresponding the B_x transition. The average angle between the base plane and B_x transition was 13°, and between the B_x and B_y transitions was 8°. Similar results were obtained from the DNA–TMPyP complexes at lower [porphyrin]/[DNA] ratios. Although these calculations are not applicable in the presence of DAPI, due to the fact that the absorption tail of the DAPI (~420 nm) duplicates that of the porphyrins, similar LD^r behavior in the Soret band of the DNA–DAPI–porphyrin complex permits the conclusion that the binding geometry of TMPyP and BMPyP is not affected by the presence of DAPI.

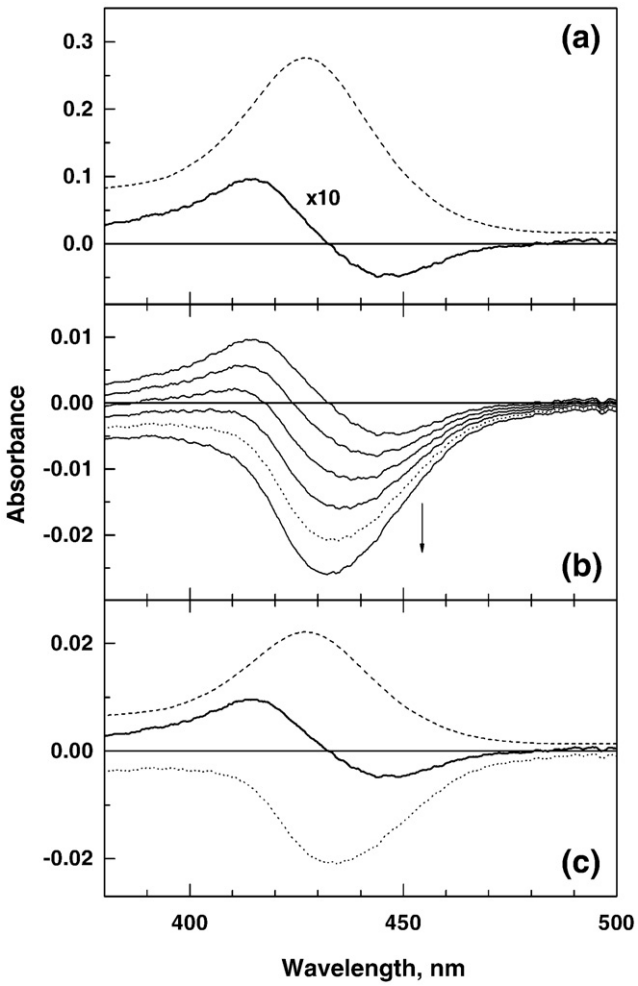

Fig. 9. (a) Absorption (dashed curve) and enlarged LD spectrum (solid curve) of the DNA–BMPyP complex in the Soret absorption region. (b) Measured LD spectrum (curve a) and stepwise reduction of the LD spectrum by absorption spectrum according to $LD(\lambda) - \kappa A(\lambda)$, where $\kappa = 0.04$, 0.06, 0.08, 0.10, and 0.12. The spectrum corresponds to $\kappa = 0.08$ (curve b, dotted curve) and is assumed to represent the pure LD of one of the electric transitions of BMPyP. (c) LD spectrum of BMPyP complexed with DNA, resolved into contributions from two transitions.

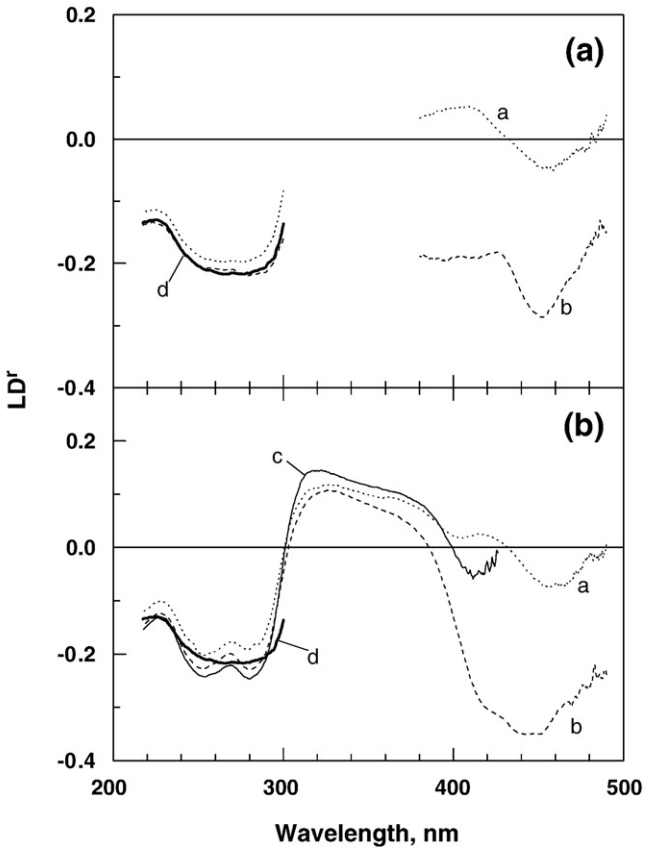

Fig. 8. LD^r spectrum of the DNA–TMPyP and –BMPyP complexes in the absence (panel a) and presence of DAPI (panel b). Curve a (dotted curve): the DNA–BMPyP complex; curve b (dashed curve): the DNA–TMPyP complex; curve d: drug-free DNA. In panel b, the LD^r spectrum of the DNA–DAPI complex is marked by curve c (solid curve). Concentrations are the same as in Fig. 7.

4. Discussion

4.1. Binding mode of TMPyP and BMPyP in the presence and absence of DAPI

The spectral properties of the DNA-bound DAPI have been reported and can be summarized as a positive CD and LD^r spectrum in the DAPI absorption region, and a large enhancement in the fluorescence intensity [23–29,42]. These spectral properties have been accepted as the signal that DAPI binds in the minor groove of DNA where the angle of the long axes of the DAPI molecule tilts 45° from the local DNA helical axis. When the DAPI molecule is inserted in the minor groove, the contact with water molecules, which is a quencher of DAPI fluorescence, is prevented. This has long been thought to be a reason for the increase in fluorescence intensity of DAPI upon binding to DNA. In the minor groove, the rotation between the phenyl and indole moieties is prevented, resulting in the preclusion of an intra-molecular charge separation between the two moieties, which also contribute to the enhancement of the fluorescence intensity [43]. In the presence of TMPyP or BMPyP, the properties of absorption, and CD and LD spectra essentially remain the same, except for the large decrease in fluorescence intensity.

Spectral properties of the DNA–TMPyP complex are characterized by a negative CD band and negative LD^r signal whose magnitude is larger or comparable with that in the DNA absorption region. All these properties are indicative of the intercalation of TMPyP between DNA base pairs. These spectral characteristics were not dependent on [porphyrin]/[DNA] ratios below 0.015, corresponding to one TMPyP per 66 bases or 33 base pairs, suggesting that the binding of TMPyP to DNA is noncooperative since if there were any cooperativity, the spectral properties would be expected to be binding ratio dependent. The characteristics of the negative CD and LD^r were unchanged, suggesting that the intercalation-binding mode of TMPyP is retained even when the minor groove is saturated with DAPI. A slight variation in the absorption spectrum may be attributed to the interaction of TMPyP with near-by DAPI. The apparent spectral properties of the BMPyP upon binding to DNA, including a zero induced CD, a bisignate LD spectrum, and the angle of the transition moments of BMPyP with respect to the local DNA helix being ~40° and 60°, are in contrast with TMPyP. From these results, the possibility of an intercalation-binding mode can be completely ruled out for the BMPyP. The minor groove-binding mode in which the crescent-shape side of the porphyrin molecule fits deep in the groove is not conceivable because the DAPI is already saturated in the same groove. It has been reported that TMPyP binds across poly[d(A-T)$_2$] and poly(dA)·poly(dT) when the minor groove is saturated by DAPI molecules [19]. However, this does not seem to be the case with BMPyP as a strong positive CD and an angle between the TMPyP's transition moments relative to the DNA helix was 48°–51° for the AT rich DNA–DAPI–TMPyP complex. This was in contrast with the ~40° and ~60°, and zero CD observed for BMPyP in this study. Furthermore, the energy transfer from DAPI to TMPyP, mediated by AT-rich DNAs, was by far more efficient due to the near contact between DAPI and TMPyP, compared to that of BMPyP. Rejecting these possibilities, BMPyP can conceivably associate with DNA in the major groove where association between BMPyP molecules is possible because the absorption spectrum depends strongly on the [porphyrin]/[DNA] ratio in the presence, as well as absence, of DAPI, even at the low mixing ratios adopted in this study. In the case of poly(dA)·poly(dT), strong evidence, that supports the stacking of TMPyP occurs in the major groove, has been reported [48].

4.2. Energy transfer

A straight line was observed in the Stern–Volmer plot of the quenching of DNA-bound DAPI by BMPyP while the decay time of DAPI was not affected, suggesting that the quenching mechanism is simply static, whereby the fluorescence of DAPI is quenched through formation of a non-fluorescent complex between DAPI and BMPyP. In the DAPI–BMPyP complex, the energy level of DAPI from which the fluorescence emits coincides with the absorption energy levels of the BMPyP and is denoted as a Förster type resonance energy transfer. Closer analysis of the Stern–Volmer plot showed that approximately 11% of the fluorescence is quenched when the DAPI concentration was 2.0 μM and BMPyP was 0.3 μM. If the efficiency of quenching is assumed to be 1, and the fluorescence of the quenchable DAPI molecule is completely quenched by BMPyP, the above concentrations correspond to an average of 0.7 DAPI molecules whose fluorescence is quenched by one BMPyP molecule. The Stern–Volmer plot for the DNA–DAPI complex by TMPyP is quite different in two aspects from the BMPyP: the shape of the quenching curve is upward, unlike the straight line observed for BMPyP; the appearance of a shortening of the average decay time. Although the shortening of decay time is usually assigned to dynamic-collisional quenching, whereby the excitation energy of a fluorophore transfers to the quencher through collision, it is not the case for the DNA–DAPI–TMPyP complex because the fluorescence decay time does not change in the presence of TMPyP when they are not simultaneously bound to DNA. Thus, it is conceivable that the observed shortening in the decay time may due to the change in a local conformation of DNA that provides a slightly different local environment for DAPI. An upward quenching curve associated with dynamic quenching is usually explained by the "sphere of action model": the quenching efficiency in the sphere is unity and the radius of the sphere is usually in a range comparable to the sum of the radii of the fluorophore and quencher [46]. A calculated sphere radius of 840 Å is, thus, unrealistically large and indicative that the static quenching of TMPyP for DNA-bound DAPI is by far more effective than that predicted by the "sphere of action model". Thus, in addition to the "sphere of action model", DNA should be assumed to provide an additional mechanism for the energy transfer in order to elucidate such observed abnormally large quenching efficiencies.

5. Conclusions

The energy of the excited DAPI is transferred to TMPyP far more efficiently than predicted by the "sphere of action model" when DAPI saturates the minor groove and TMPyP intercalates DNA. Nonetheless, the energy transfer from DAPI is less effective when BMPyP is conceivably associated in the major groove.

Acknowledgement

This work was supported by the Korea Science and Engineering Foundation (Grant no. R01-2008-000-20704-0).

References

[1] G.B. Schuster, Long-range charge transfer in DNA: transient structural distortions control the distance dependence, Acc. Chem. Res. 33 (2000) 253–260.
[2] B. Giese, Long-distance electron transfer through DNA, Annu. Rev. Biochem. 71 (2002) 51–70.
[3] B. Giese, Electron transfer in DNA, Curr. Opin. Chem. Biol. 6 (2002) 612–618.
[4] H.-A. Wagenknecht, Reductive electron transfer and transport of excess electrons in DNA, Angew. Chem. Int. Ed. 42 (2003) 2454–2460.
[5] F.D. Lewis, DNA molecular photonics, Photochem. Photobiol. 81 (2005) 65–72.
[6] H.-A. Wagenknecht, Electron transfer processes in DNA: mechanisms, biological relevance and applications in DNA analytics, Nat. Prod. Rep. 23 (2006) 973–1006.
[7] E.M. Boon, J.K. Barton, Charge transport in DNA, Curr. Opin. Struct. Biol. 12 (2002) 320–329.
[8] M.E. Núñez, G.P. Holmquist, J.K. Barton, Evidence for DNA charge transport in the nucleus, Biochemistry 40 (2001) 12465–12471.
[9] M.E. Núñez, K.T. Noyes, J.K. Barton, Oxidative charge transport through DNA in nucleosome core particles, Chem. Biol. 9 (2002) 403–415.
[10] C.J. Murphy, M.R. Arkin, Y. Jenkins, N.D. Ghatlia, S. Bossmann, N.J. Turro, J.K. Barton, Long-range photoinduced electron transfer through a DNA helix, Science 262 (1993) 1025–1029.

[11] C.J. Murphy, M.R. Arkin, N.D. Ghatlia, S. Bossmann, N.J. Turro, J.K. Barton, Fast photoinduced electron transfer through DNA intercalation, Proc. Natl. Acad. Sci. U. S. A. 91 (1994) 5315–5319.
[12] D. Garcia-Fresnadillo, N. Boutonnet, S. Schumm, C. Moucheron, A. Kirsch-De Mesmaeker, E. Defrancq, J.F. Constant, J. Lhomme, Luminescence quenching of Ru-labeled oligonucleotides by targeted complementary strands, Biophys. J. 82 (2002) 978–987.
[13] T. Takada, K. Kawai, S. Tojo, T. Majima, Hole transfer in DNA: DNA as a scaffold for hole transfer between two organic molecules, Tetrahedron Lett. 44 (2003) 3851–3854.
[14] V.D. Lakhno, V.B. Sultanov, B.M. Pettitt, Combined hopping–superexchange model of a hole transfer in DNA, Chem. Phys. Lett. 400 (2004) 47–53.
[15] J. Rak, J. Makowska, A.A. Voityuk, Effect of proton transfer on the electronic coupling in DNA, Chem. Phys. 325 (2006) 567–574.
[16] A. Sadowska-Aleksiejew, J. Rak, A.A. Voityuk, Effects of intra base-pairs flexibility on hole transfer coupling in DNA, Chem. Phys. Lett. 429 (2006) 546–550.
[17] B.W. Lee, S.J. Moon, M.R. Youn, J.H. Kim, H.G. Jang, S.K. Kim, DNA mediated resonance energy transfer from 4′,6-diamidino-2-phenylindole to $[Ru(1,10\text{-Phenanthroline})_2L]^{2+}$, Biophys. J. 85 (2003) 3865–3871.
[18] B.W. Yun, J.-O. Kim, B.W. Lee, P. Lincoln, B. Nordén, J.-M. Kim, S.K. Kim, Simultaneous binding of Ruthenium(II) $[(1,10\text{-phenanthroline})_2$dipyridophenazine$]^{2+}$ and minor groove binder 4′,6-diamidino-2-phenylindole to poly[d(A-T)$_2$] at high binding densities: observation of fluorescence resonance energy transfer across the DNA stem, J. Phys. Chem. B. 107 (2003) 9858–9864.
[19] B. Jin, H.M. Lee, Y.-A. Lee, J.H. Ko, C. Kim, S.K. Kim, Simultaneous binding of *meso*-tetrakis(*N*-methylpyridinium-4-yl)porphyrin and 4′,6-diamidino-2-phenylindole at the minor grooves of poly(dA)·poly(dT) and poly[d(A-T)$_2$]: fluorescence resonance energy transfer between DNA bound drugs, J. Am. Chem. Soc. 127 (2005) 2417–2424.
[20] M.R. Youn, S.J. Moon, B.W. Lee, D.-J. Lee, J.-M. Kim, S.K. Kim, C.-S. Lee, DNA mediated energy transfer from 4′,6-diamidino-2-phenylindole to Ru(II)$[(1,10\text{-phenanthroline})_2L]^{2+}$: effect of ligand structure, Bull. Korean Chem. Soc. 26 (2005) 537–542.
[21] J.Y. Choi, J.-M. Lee, H. Lee, M.J. Jung, S.K. Kim, J.-M. Kim, Mixing ratio-dependent energy transfer from DNA-bound 4′,6-diamidino-2-phenylindole to $[Ru(1,10\text{-phenanthroline})_2$dipyrido[3,2-*a*:2′,3′-*c*]phenazine$]^{2+}$, Biophys. Chem. 134 (2008) 56–63.
[22] S. Erkisson, S.K. Kim, M. Kubista, B. Nordén, Binding of 4′,6-diamidino-2-phenylindole (DAPI) to AT regions of DNA: evidence for an allosteric conformational change, Biochemistry 32 (1993) 2987–2998.
[23] H.-K. Kim, J.-M. Kim, S.K. Kim, A. Rodger, B. Nordén, Interactions of intercalative and minor groove binding ligands with triplex poly(dA)·[poly(dT)]$_2$ and with duplex poly(dA)·poly(dT) and poly[d(A-T)]$_2$ studied by CD, LD, and normal absorption, Biochemistry 35 (1996) 1187–1194.
[24] T.A. Larsen, D.S. Goodsell, D. Cascio, K. Grzeskowiak, R.E. Dickerson, The structure of DAPI bound to DNA, J. Biomol. Struct. Dyn. 7 (1989) 477–491.
[25] S. Mohan, N. Yathindra, Flexibility of DNA in 2:1 drug–DNA complexes—simultaneous binding of two DAPI molecules to DNA, J. Biomol. Struct. Dyn. 9 (1991) 695–704.
[26] E. Trotta, E. D'Ambrosio, N. Del Grosso, G. Ravagnan, M. Cirilli, M. Paci, 1H NMR study of [d(GCGATCGC)]$_2$ and its interaction with minor groove binding 4′,6-diamidino-2-phenylindole, J. Biol. Chem. 268 (1993) 3944–3951.
[27] D. Vlieghe, J. Sponer, L. Van Meervelt, Crystal structure of d(GGCCAATTGG) complexed with DAPI reveals novel binding mode, Biochemistry 38 (1999) 16443–16451.
[28] L.G. Marzilli, L.D. Banville, G. Zon, W.D. Wilson, Pronounced proton and phosphorus-31 NMR spectral changes on *meso*-tetrakis(*N*-methylpyridinium-4-yl)porphyrin binding to poly[d(G-C)]poly[d(G-C)] and to three tetradecaoligodeoxyribonucleotides: evidence for symmetric, selective binding to 5′CG3′ Sequences, J. Am. Chem. Soc. 108 (1986) 4188–4192.
[29] A.B. Guliaev, N.B. Leontis, Cationic 5,10,15,20-tetrakis(*N*-methylpyridinium-4-yl) porphyrin fully intercalates at 5′-CG-3′ steps of duplex DNA in solution, Biochemistry 38 (1999) 15425–15437.
[30] U. Sehlstedt, S.K. Kim, P. Carter, J. Goodisman, J.F. Vollano, B. Nordén, J.C. Dabrowiak, Interaction of cationic porphyrins with DNA, Biochemistry 33 (1994) 417–426.
[31] B.H. Yun, S.H. Jeon, T.-S. Cho, S.Y. Yi, U. Sehlstedt, S.K. Kim, Binding mode of porphyrins to poly[d(A-T)$_2$] and poly[d(G-C)$_2$], Biophys. Chem. 70 (1998) 1–10.
[32] S. Lee, S.H. Jeon, B.-J. Kim, S.W. Han, H.G. Jang, S.K. Kim, Classification of CD and absorption spectra in the Soret band of H_2TMPyP bound to various synthetic polynucleotides, Biophys. Chem. 92 (2001) 35–45.
[33] M.A. Sari, J.P. Battioni, D. Dupre, D. Mansuy, J.B. Le Pecq, Cationic porphyrin–DNA interactions: importance of the number and position of the charges, Biochem. Pharmacol. 37 (1988) 1861–1862.
[34] E.J. Gibbs, I. Tinoco Jr., M.F. Maestre, P.A. Ellinas, R.F. Pasternack, Self-assembly of porphyrins on nucleic acid templates, Biochem. Biophys. Res. Commun. 157 (1988) 350–358.
[35] M. Ismail, P.M. Rodger, A. Rodger, Drug self-assembly on DNA: sequence effects with *trans*–*bis*-(4-*N*-methylpyridiniumyl)diphenyl porphyrin and Hoechst 33258, J. Biomol. Struct. Dyn. Conversation 11 (2000) 335–348.
[36] J.R. Lakowiz, Principles of Fluorescence Spectroscopy, 2nd ed., Plenum Press, New York, 2001, pp. 237–265.
[37] B. Nordén, M. Kubista, T. Kurucsev, Q. Rev. Biophys. Chem. 25 (1992) 51–170.
[38] B. Nordén, T. Kurucsev, Analysing DNA complexes by circular and linear dichroism, J. Mol. Recognit. 7 (1994) 141–156.
[39] A. Rodger, B. Nordén, Circular Dichroism & Linear Dichroism, Oxford University Press, New York, 1997.
[40] A. Wada, S. Kozawa, Instrument for the studies of differential flow dichroism of polymer solutions, J. Polym. Sci. 2 (1964) 853–864.
[41] J. Kapuscinski, B. Skoczylas, Simple and rapid fluorimetric method for DNA microassay, Anal. Biochem. 83 (1977) 252–257.
[42] B. Nordén, S. Erkisson, S.K. Kim, M. Kubista, R. Lyng, B. Åkerman, in: B. Pullman, J. Jortner (Eds.), Molecular Basis of Specificity in Nucleic Acid–Drug Interactions, Kluwer Acad. Pub., Netherlands, 1990, pp. 23–41.
[43] A.G. Szabo, D.T. Krajcarski, P. Cavatorta, L. Masotti, M.L. Barcellona, Excited state pK_a behavior of DAPI. A rationalization of the fluorescence enhancement of DAPI in DAPI–nuclecic acid complexes, Photochem. Photobiol. 44 (1986) 143–150.
[44] P. Cavatorta, L. Masotti, A.G. Szabo, A time-resolved fluorescence study of 4′,6′-diamidine-2-phenylindole dihydrochloride binding to polynucleotides, Biophys. Chem. 22 (1985) 11–16.
[45] M.L. Barcellona, E. Gratton, Fluorescence lifetime distributions of DNA-4′,6-diamidino-2-phenylindole complex, Biochim. Biophys. Acta 993 (1989) 174–178.
[46] E. Casali, P.H. Petra, J.B.A. Ross, Fluorescence investigation of the sex steroid binding protein of rabbit serum: steroid binding and subunit dissociation, Biochemistry 29 (1990) 9334–9343.
[47] Y.-A. Lee, S. Lee, T.-S. Cho, C. Kim, S.W. Han, S.K. Kim, Binding mode of *meso*-tetrakis(*N*-methylpyridinium-4-yl)porphyrin to poly[d(I-C)$_2$]: effect of amino group at the minor groove of poly[d(G-C)$_2$] on the porphyrin–DNA interaction, J. Phys. Chem., B 106 (2002) 11351–11355.
[48] Y.-A. Lee, J.-O. Kim, T.-S. Cho, R. Song, S.K. Kim, Binding of *meso*-tetrakis(*N*-methylpyridium-4-yl)porphyrin to triplex oligonucleotides: evidence for the porphyrin stacking in the major groove, J. Am. Chem. Soc. 125 (2003) 8106–8107.